Laser and Particle Beams

cambridge.org/lpb

Evolution of magnetic field in a weakly relativistic counterstreaming inhomogeneous e^-/e^+ plasmas

Sandeep Kumar[1], Y. K. Kim[2], T. Kang[2], Min Sup Hur[2] and Moses Chung[2]

[1]Department of Physics, Manav Rachna University (MRU), Faridabad, Haryana, India and [2]Department of Physics, Ulsan National Institute of Science and Technology, Ulsan, South Korea

Research Article

Cite this article: Kumar S, Kim YK, Kang T, Hur MS, Chung M (2020). Evolution of magnetic field in a weakly relativistic counterstreaming inhomogeneous e^-/e^+ plasmas. *Laser and Particle Beams* 1–7. https://doi.org/10.1017/S0263034620000233

Received: 29 May 2020
Revised: 7 June 2020
Accepted: 29 June 2020

Key words:
Gamma-ray burst; magnetic field; plasma instabilities; temperature anisotropy

Author for correspondence: M. Chung and M. S. Hur, Department of Physics, Ulsan National Institute of Science Technology, Ulsan, South Korea.
E-mail: mchung@unist.ac.kr; mshur@unist.ac.kr

Abstract

The nonlinear evolution of electron Weibel instability in a symmetric, counterstream, unmagnetized electron–positron e^-/e^+ plasmas is studied by a 2D particle-in-cell (PIC) method. The magnetic field is produced and amplified by the Weibel instability, which extracts energy from the plasma anisotropy. A weakly relativistic drift velocity of $0.5c$ is considered for two counterstreaming e^-/e^+ plasma flows. Simulations show that in a homogeneous e^-/e^+ plasma distribution, the magnetic field amplifies exponentially in the linear regime and rapidly decays after saturation. However, in the case of inhomogeneous e^-/e^+ plasma distribution, the magnetic field re-amplifies at post-saturation. We also find that the amount of magnetic field amplification at post-saturation depends on the strength of the density inhomogeneity of the upstream plasma distribution. The temperature calculation shows that the finite thermal anisotropy exists in the case of an inhomogeneous plasma distribution which leads to the second-stage magnetic field amplification after the first saturation. Such density inhomogeneities are present in a variety of astrophysical sources: for example, in supernova remnants and gamma-ray bursts. Therefore, the present analysis is very useful in understanding these astrophysical sources, where anisotropic density fluctuations are very common in the downstream region of the relativistic shocks and the widely distributed magnetic field.

Introduction

Electromagnetic instabilities like Weibel instability (Weibel, 1959) and filamentation instability (Fried, 1959) owing to their self-generated fields play a very important role in high-energy astrophysical phenomena such as particle acceleration and synchrotron emission. These instabilities are widely investigated (Kalman *et al.*, 1968; Davidson *et al.*, 1972; Califano *et al.*, 1998; Silva *et al.*, 2002; Bret, 2006; Rowlands *et al.*, 2007) and being applied in several astrophysical scenarios, such as cosmic rays (Lucek and Bell, 2000), supernova remnants (SNRs), and jets from active galactic nuclei (AGN) (Medvedev and Loeb, 1999; Nishikawa *et al.*, 2003; Medvedev *et al.*, 2005; Spitkovsky, 2008; Ardaneh *et al.*, 2015), and in laser–plasma experiments (Fiuza *et al.*, 2012; Fox *et al.*, 2013).

These instabilities release the excess of free energy stored in the plasma particle anisotropy, residing, for example, in a temperature anisotropy or in a counterstreaming motion of the plasma. A substantial fraction of the kinetic energy of plasma particles is converted into the magnetic energy generation and its amplification by these instabilities (Califano *et al.*, 1998). The processes leading to the magnetic field generation in the intergalactic medium has been treated as an unsolved problem and remained a matter of debate (Kronberg, 2002). Therefore, understanding the evolution of these instabilities in both its linear and nonlinear phases and the prediction of the amplitude of the Weibel-generated magnetic fields are of primary importance for a deeper insight into various astrophysical events, as well as laser–plasma related studies. Among several astrophysical scenarios, SNRs are ubiquitous and routinely observed in radio to gamma X-ray bands. X-ray observations have shown that electrons are accelerated to highly relativistic energies in SNR shocks (Nishikawa *et al.*, 2003). The X-ray observations of SNRs suggest the magnetic field amplification up to 10^{-2}–10^{-3} μG in the vicinity of the collisionless shock front (Berezhko *et al.*, 2003*a*, 2003*b*; Vink and Laming, 2003; Bamba *et al.*, 2005; Uchiyama *et al.*, 2007).

The presence of amplified magnetic fields in young SNR is well acknowledged now. However, Gamma Ray Bursts (GRBs) and AGN require a stronger magnetic field that cannot be achieved by shock compression solely. Various mechanisms have been proposed for magnetic field amplification in different astrophysical environments, some of them are cosmic ray-driven instability, whereby cosmic rays diffuse to the upstream region where the resonant and the nonresonant instabilities become unstable and cause fluctuations in the magnetic field (Bell, 2004; Reville *et al.*, 2006, 2007). The nonresonant instability has been investigated with

particle-in-cell (PIC) simulations (Niemiec *et al.*, 2008; Riquelme and Spitkovsky, 2008; Ohira *et al.*, 2009).

Nonetheless, the detailed physics of such wide magnetic field generations is still uncertain. It is assumed that the leading hypothesis for field amplification in GRB afterglows of SNRs is the relativistic Weibel instability (Medvedev and Loeb, 1999) where the instability extracts free energy from the anisotropy of the particles, and produces filamentary currents aligned with the normal direction; and these currents are responsible for the creation of transverse magnetic fields.

Furthermore, the extensive distributions of the magnetic field energy in GRBs put forward that including the microphysics, macroscopic properties of GRB environments are equally important for the generation of magnetic fields. Therefore, GRBs and their surrounding environment are poorly known. Among macroscopic structures present, there should be clump wind regions and shocked wind regions in the surrounding environments of GRBs. Each GRB is different in their structures and length scales. Moreover, the observational evidence of radio waves shows the electron density irregularities over a wide range of scale size of the interstellar medium (ISM), and the Kolmogorov power spectrum justifies the existence of large-scale density turbulence (Lee and Jokipii 1976; Armstrong *et al.*, 1981; Armstrong *et al.*, 1995).

Sironi *et al.* have proposed the magnetic field amplification through macroscopic turbulence excited by the interaction of the shock with a clumpy pre-shock medium (Sironi and Goodman, 2007). Theoretical estimations made for intergalactic plasmas also suggest micro-Gauss levels of the magnetic field of Weibel type which are consistent with the magnetic field values 10^{-7}–10^{-5} G derived from Faraday rotation measure of the linearly polarized emission of galactic or extragalactic sources (Lazar *et al.*, 2009*a*). Recently (Tomita and Ohira, 2016), the second-stage magnetic field amplification is observed on the basis of Weibel-type plasma instability which is driven by density fluctuations.

Counterstreaming plasma systems with intrinsic temperature anisotropies are susceptible to the excitation of Weibel- and filamentation-type instabilities and are extensively studied in the homogeneous plasma medium (Bret and Deutsch 2006; Lazar *et al.*, 2006, 2008, 2009*b*; Stockem and Lazar, 2008; Stockem *et al.*, 2009; Bret *et al.*, 2016; Dieckmann and Bret 2017, 2018). Here, we study the electron Weibel instability induced in weakly relativistic counterstreaming plasmas with the inhomogeneous distribution and with intrinsic anisotropies and compare with widely studied counterstreaming plasmas with homogeneous distribution. As mentioned earlier, in SNRs and in GRBs, such inhomogeneous outflows are always present and we can expect some role of the Weibel instability/filamentation instability. Therefore, in the context of SNRs and GRBs, it is shown using PIC simulation that the pre-shock density distribution plays an important role in the magnetic field generation. Moreover, such small-scale inhomogeneity also exits in the intracluster medium (ICM) and the circumstellar medium (CSM) which may further trigger the magnetic field after saturation in the downstream region of the relativistic shock. Numerical PIC simulations have been used to describe the dynamics of a region corresponding to the downstream of the shock, in which the upstream inhomogeneous plasma has been compressed along the shock propagation direction. The computational plasma domain is considered relatively smaller compared to the long-scale domain of the density fluctuations present in astrophysical environments.

In Section "Numerical method and code resolution", we present the numerical method and code resolution. In Section "Simulation results", we present the simulation results on Weibel instability, associated growth of the magnetic field components and resulting in the magnetic energy development. We also discuss the thermal anisotropy development for the e^-/e^+ plasmas with homogeneous and inhomogeneous density distributions. Finally, the conclusion is presented in the section "Conclusion".

Numerical method and code resolution

For our simulation, we consider the pre-existing isotropic plasma density fluctuations and study the probable effects on the downstream motion and its characteristics. First, we consider two symmetric counterstreaming electron–positron e^-/e^+ plasma flows with initial drift velocities, $\vec{v}_0 = \pm v_0 \hat{y}$ with $v_0 = 0.5c(\gamma_0 \cong 1)$, that is, a weakly relativistic case. Each e^-/e^+ plasma has the same density and the thermal velocity is equivalent to $v_{\rm th} = 0.1c$ along the $\hat{y}$ direction. The initial particle distribution is Maxwellian and the initial conditions of the flows are unstable for the Weibel instability. Two different plasma distributions, $n(x, y)$ are considered: the first is the spatially uniform homogeneous plasma; $n(x, y) = n_0$, and the second is the inhomogeneous plasma distribution which is closer to the reality and is of the form of $n(x, y) = n_0[1 + \delta n/n_0 \sin(2\pi x/L_x)]$, where $\delta n/n_0$ is the amplitude of the density fluctuation, n_0 is the constant electron number density, and L_x is the simulation box size along the $\hat{x}$ direction. The system has initially zero net current. The simulation box length is normalized by $c/\omega_{\rm pe}$ and the wavenumber by $\omega_{\rm pe}/c$, where c is the speed of light in vacuum and $\omega_{\rm pe} = \sqrt{n_0 e^2/m_e \epsilon_0}$ is the electron plasma frequency. Here, m_e and e are the electron rest mass and charge, respectively.

To understand the magnetic field amplifications, PIC simulations are carried out using EPOCH (Arber *et al.*, 2015) code and cplPIC (Hur and Suk, 2011; Cho *et al.*, 2015) code. In PIC simulations, the interplay of the electric and magnetic fields with the particles of a collisionless kinetic plasma is modeled self-consistently. The main set of equations associated with PIC codes are the Lorentz force as the equation of motion, and the Maxwell's equations determining the electric and magnetic fields. In our simulations, the cell size $\Delta x = \Delta y = 0.1c/\omega_{\rm pe}$ and the simulation time step $\Delta t = 0.05\omega_{\rm pe}^{-1}$ are considered, respectively. The simulation domain $L_x \times L_y = 128c/\omega_{\rm pe} \times 128c/\omega_{\rm pe}$ is chosen for this study and periodic boundary conditions are used. The initial density of the e^-/e^+ particles per cell is 40. Each cell contains 40 electrons and 40 positrons on average.

Simulation results

Evolution of magnetic field energy and its saturation

For the electric and the magnetic field energy calculation, the box-averaged energies of the electric $E_i(x, y, t)$ and $B_i(x, y, t)$ field components are given by $\epsilon_{E_i}(t) = (N_x N_y)^{-1} \sum_{j,k} \epsilon_0 [E_i(j\Delta_x, k\Delta_x, t)]^2/2$ and $\epsilon_{B_i}(t) = (N_x N_y)^{-1} \sum_{j,k} [B_i(j\Delta_x, k\Delta_x, t)]^2/2\mu_0$, respectively. The box-averaged kinetic energy density is $\epsilon_K(t) = (N_x N_y)^{-1} \sum_j m_{\rm cp} c^2(\gamma_j - 1)$ in our 2D PIC simulation.

Figure 1a shows energies corresponding to E_x, E_y along with B_z components for the inhomogeneous distribution case for $\delta n/n_0 = 0.75$. The B_z is the only component that grows in the considered geometry in response to the Weibel instability and the magnitude of E_x, E_y energies is lower than B_z energy. Figure 1b demonstrates the time evolution of the box-averaged energies of B_z component for the counterstreaming e^-/e^+ plasmas. For a

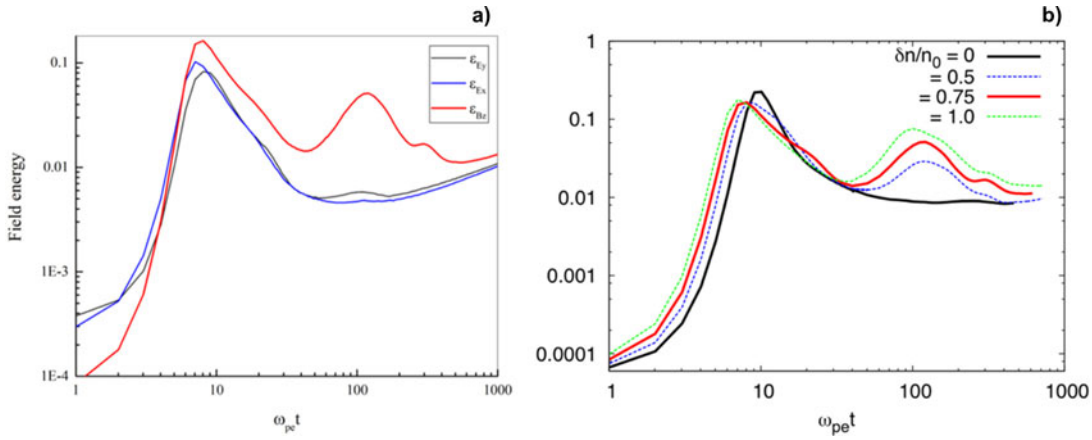

Fig. 1. (a) The logarithmic plot of the temporal evolution of the field energies of E_x, E_y, and B_z for $\delta n/n_0 = 0.75$. (b) The logarithmic plot of the temporal evolution of the transverse magnetic field energy (B_z component) for different plasma density inhomogeneities: $\delta n/n_0 = 0$ (black line), 0.5 (blue-dotted line), 0.75 (red line), and 1.0 (green-dotted line), respectively.

homogeneous plasma case (black line), the amplified energy of B_z shows exponential growth in the linear regime up to $t \sim 10\omega_{pe}^{-1}$. However, in the nonlinear regime, the magnetic energy simply decays which is similar to the previous findings (Tomita and Ohira, 2016; Grassi *et al*, 2017). While in an inhomogeneous plasma case (blue line, red line, and green line), the magnetic energy of B_z initially shows similar behavior in the linear stage as in the case of homogeneous plasma. However, after the saturation at $t \sim 10\omega_{pe}^{-1}$, magnetic energy of B_z again gets amplified around $t \sim 270\omega_{pe}^{-1}$ (blue-dotted line) for $\delta n/n_0 = 0.5$. Hence, the magnetic field is amplified for longer time in the inhomogeneous e^-/e^+ plasmas even though the total kinetic energy is the same as in the case of the homogeneous e^-/e^+ plasmas. To confirm this result, we examine simulations with different density inhomogeneities, $\delta n/n_0 = 0.75$ (red line) and 1.0 (green-dotted line), respectively. We find similar growth of the magnetic energy with enhanced magnitude at the second peak as shown in Figure 1b.

Such an inhomogeneous plasma distribution is commonly found in GRBs where isotropic density fluctuations post-shock becomes anisotropic in the shock transition region. Finally, these distributions cause anisotropy in velocity distributions as well in the downstream region due to the temperature anisotropy (Tomita and Ohira, 2016). However, the scale of the plasma environment for GRBs are on much larger scales than the plasma scale considered here in the simulation. Therefore, large-scale simulations are required to confirm the above scaling which is impossible in PIC simulation.

Figures 2a and 2b show the 2D profile of the magnetic field B_z, component at two different simulation times $t \sim 10\omega_{pe}^{-1}$ and $t \sim 270\omega_{pe}^{-1}$, respectively, in the inhomogeneous e^-/e^+ plasma case. From Figure 2a, one can notice that in the beginning, small magnetic filaments are developed only in a high-density region, $0 < x/c\omega_{pe}^{-1} < 60$, that is, left-hand side of the simulation domain. Whereas, in the right-hand side of the simulation domain $60 < x/c\omega_{pe}^{-1} < 126$, magnetic filaments are completely absent. However, at $t \sim 270\omega_{pe}^{-1}$as shown in Figure 2b, the previous smaller structures on the left-hand side of the simulation domain, grow with time and form large-scale magnetic structures along the counterstreaming e^-/e^+ plasmas flow direction $\hat{y}$. Interestingly, on the right-hand side of the simulation box, $60 < x/c\omega_{pe}^{-1} < 126$, which is a low-plasma density region, the magnetic field structures with finite magnitude and finite scale appear along the $\hat{x}$ direction. Therefore, we find that the magnetic field fluctuations start to grow after the saturation of the first Weibel instability. As mentioned earlier, there is no net magnetic field in the right-hand side of the simulation domain at $t = 0$. Therefore, the second growth of the magnetic field is also expected to be due to Weibel instability. The Fourier spectrums corresponding to Figures 2a and 2b are shown in Figures 2c and 2d, respectively. One can see that the larger values of k_x and k_y of B_z shown in Figure 2c confirm that the shortest magnetic field structures are produced in the initial simulation stage at $t \sim 10\omega_{pe}^{-1}$. Similarly, Figure 2d represents the Fourier spectrum corresponding to Figure 2b, which shows the smaller values of k_x and k_y of B_z. This means larger magnetic structures are developed nearby $t \sim 270\omega_{pe}^{-1}$.

Weibel instability due to thermal anisotropy generation

In this section, we study the evolution of temperature anisotropy $A = (T_y/T_x - 1)$ in homogeneous and inhomogeneous plasma distributions both which is shown in Figure 3. The A is an important parameter to understand the magnetic field amplification *via* anisotropic density fluctuations present in the downstream region of the shock in GRBs. The A is calculated with the simulation time by taking averages of electron momentum components p_x and p_y over the whole simulation domain along the simulation time. At $t = 0$, the counterstreaming e^-/e^+ plasmas have finite thermal temperature $T_y > T_x$ along the $\hat{y}$ direction only. This initial anisotropic velocity distribution, $v_{thy} = 0.1c$ and $v_{thx} = 0$, makes the system Weibel unstable.

For these initial conditions, for the homogeneous plasma distribution in the simulation box $0 < x < 128c/\omega_{pe}$, thermal anisotropy A (black line) starts decreasing from its maximum value, and finally approaches toward zero as the simulation progresses with time. The system is isotropized slowly with the simulation time. However, in the inhomogeneous plasma distribution case, shown for $\delta n/n_0 = 0.5$, A (blue line) shows a similar variation initially, however, different in magnitude. As the simulation time grows, it shows later oscillatory pattern post-saturation and becomes negative in the downstream region. The size of these oscillation becomes larger. The similar pattern was observed for 0.75 (cyan line) and 1.0 (red line), respectively. The inset of

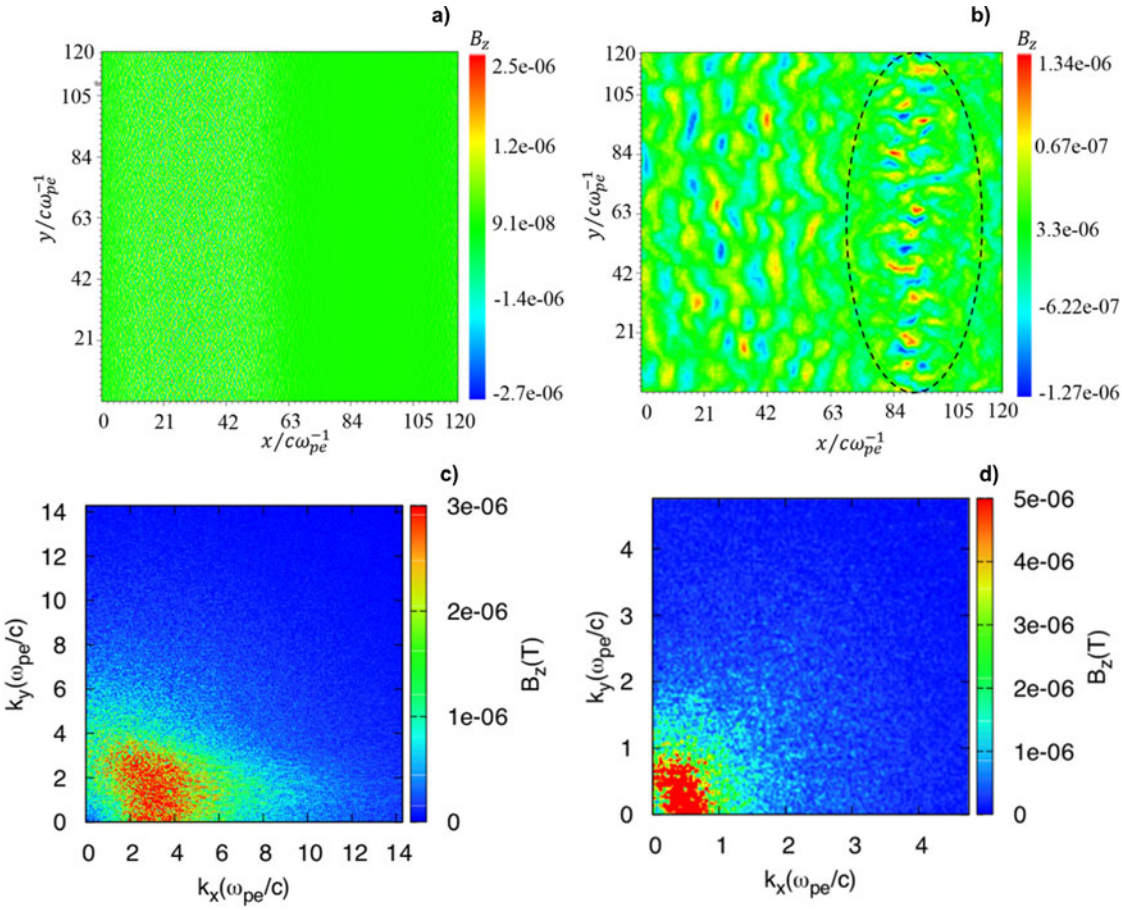

Fig. 2. 2D snapshots of the B_z component in an inhomogeneous e^-/e^+ plasma system at two different simulation times: (a) at $0 < x < 128c/\omega_{pe}$ and (b) at $0 < x < 128c/\omega_{pe}$ and the corresponding k-spectra of B_z: (c) at $t \sim 270\omega_{pe}^{-1}$ and (d) at $t \sim 270\omega_{pe}^{-1}$, respectively.

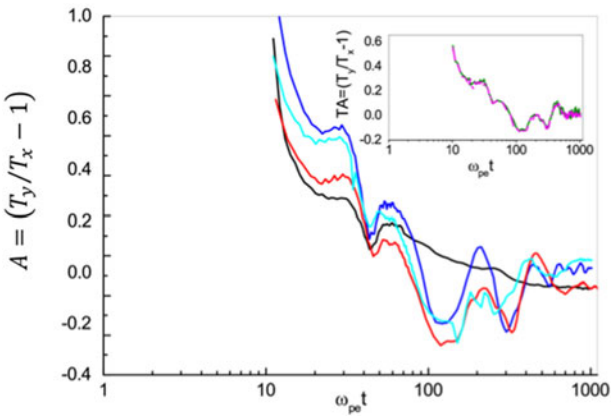

Fig. 3. The evolution of temperature anisotropy $A = (T_y/T_x - 1)$ along the simulation time for different plasma density inhomogeneities: $\delta n/n_0 = 0$ (black line), 0.5 (blue line), 0.75 (cyan line), and 1.0 (red line), respectively.

Figure 3 shows the temperature anisotropy temperature anisotropy (TA) along the simulation time for the $\delta n/n_0 = 0.75$ case in the high-plasma density region, $20c/\omega_{pe} < x < 42c/\omega_{pe}$ (purple line), and in the low-plasma density region, $80c/\omega_{pe} < x < 110c/\omega_{pe}$ (cyan line). Both TA curves show similar oscillator patterns as the plasma is isotropized by the magnetic field; however, the scale length is relatively smaller.

As mentioned earlier, the simulation domain length used here is relatively shorter than the scale length of the density clumps present in SNRs, ICM, and CSMs where high-density clumps with uneven scale length are supposed to be always present. These clumps are strongly compressed by the collisionless shocks by the factor Γ_d/r (Tomita and Ohira, 2016) in the normal direction (in our case, it is the $\hat{x}$ direction) at the downstream rest frame, where r and Γ_d stand for the shock compression ratio and the Lorentz factor of the downstream flow at the shock rest frame, respectively.

In this study, where the initial magnetic field is zero, the Weibel instability becomes the main driver for the magnetic field fluctuations and dissipates the upstream bulk flow in the shock transition region, so that the upstream plasma is heated isotopically. At post-shock, electrons with a large v_x escape from the high-density clump in the $\hat{x}$ direction, but it takes longer time to escape in the shock-tangential direction, that is, $\hat{y}$-axis. As a result, a temperature anisotropy appears at the high-density clump in the downstream region. Therefore, in the high-density clump, the temperature in the shock normal direction becomes lower than that in the shock-tangential direction. On the other hand, outside the high-density clump, the temperature in the shock normal direction becomes higher than that in the shock-tangential direction because there are escaping particles with a large v_x. Hence, the upstream density fluctuations generate the temperature anisotropy in the shock downstream region.

To understand the Weibel instability due to temperature anisotropy, the dispersion relation for the linear phase is given

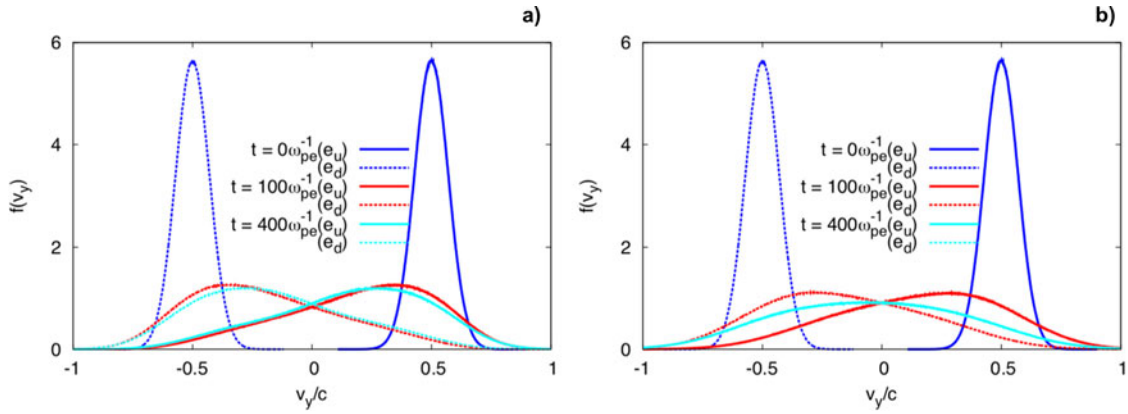

Fig. 4. The velocity distributions of counterstream electrons computed by the simulations at three different simulation time settings: $t \sim 0\omega_{pe}^{-1}$, $t \sim 100\omega_{pe}^{-1}$, and $t \sim 400\omega_{pe}^{-1}$, respectively, in (a) homogeneous and (b) inhomogeneous e^-/e^+ plasmas. Here, e_u denotes electrons motion along the $+\hat{y}$ and e_d denotes electrons motion along the $-\hat{y}$ direction.

by $k^2 + \sigma^2 = -[1 + 1/2[1 + A + 2(v_0/v_{th\perp})^2]Z'(i\sigma/kv_{th\perp})]$ (Lazar, 2008; Stockem *et al.*, 2009), where $\omega = i\sigma$, and $Z'(\zeta) = -2[1 + \zeta Z(\zeta)]$ is the first derivative of the well-known plasma dispersion function $Z(\zeta) = \pi^{-1/2}\int_{-\infty}^{\infty} d\exp(-t^2)/(t-\zeta)$ with $\zeta = \omega/kv_{th\perp}$ (Fried and Conte, 1961). For small temperature anisotropy $A \ll 1$, the maximum growth of Weibel instability can be deduced as $\gamma_{max} = (4/27\pi)^{1/2}[A^{3/2}/(1+A)](v_{th}/c)\omega_{pe}$ for $k = (A^{1/3})\omega_{pe}/c$ (Davidson *et al.*, 1972), where k is the wave vector of the most unstable mode and parallel to the direction of the lower temperature. For $A = 0.3$ and $v_{th} = 0.5c$, the mode with $k \approx 0.3\omega_{pe}/c$ shows the maximum growth rate of $\gamma_{max} \approx 10^{-2}\omega_{pe}$, directly proportional to the plasma density ω_{pe}, and closely match with our simulations.

In continuation to the discussion of the temperature anisotropy, Figure 4 shows the velocity distribution from the linear stage to the nonlinear one. The initial velocity distribution of counterstream electrons is in equilibrium state free-from external forces that is, the Maxwellian distribution centered around the velocity $v_0 = 0.5c$ (blue line and blue-dotted line) computed at time $t \sim 0\omega_{pe}^{-1}$ [see Figs. 4(a) and 4(b)]. However, as the simulation time grows, the magnetic field generates and the plasma distribution becomes anisotropic. Hence, the velocity dispersion occurs and we get the shifted Maxwellian velocity distribution at $t \sim 100\omega_{pe}^{-1}$ (red line and red-dotted line). This analysis of the electron velocity distributions in the self-generated fields initially shows that more deviations from the forward-directed motion occur only after field saturation. One can notice as the simulation time grows, the width of the velocity distribution keeps increasing and it is isotropized (cyan line and cyan-dotted line) near zero velocity at $t \sim 400\omega_{pe}^{-1}$ in the inhomogeneous case [Fig. 4(b)]. However, in the case of the homogeneous plasma, the isotropized mechanism takes much longer time.

To check the authenticity of the previous simulation results, shown in Figure 5, we show the plots of $-\hat{y}$ averaged, normalized plasma density distribution along the $\hat{x}$ direction at four different simulation time settings. The black line represents the initial density distribution at $t = 0$ which is clearly a sinusoidal variation. The red line shows the plasma density distribution taken at time $t \sim 110\omega_{pe}^{-1}$, just after the second peak of the magnetic field energy plot (see Fig. 1). Therefore, the large-scale sinusoidal density distribution turns out on a small-scale density filamentation, approaching toward the equilibration state. The electrons from the high-density region move toward the low-density region making the system in the equilibration state. The blue line taken at

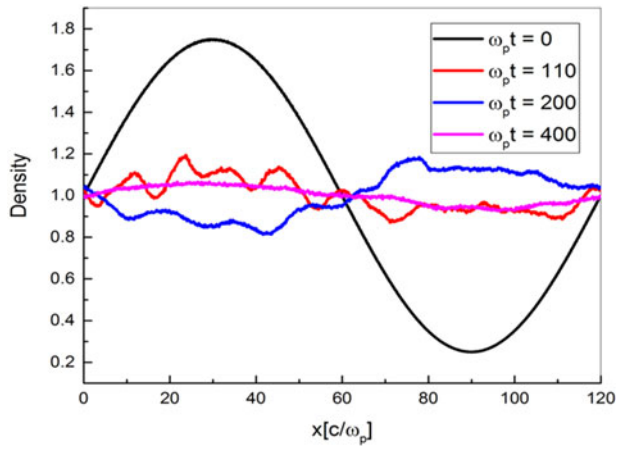

Fig. 5. Plots of the $-y$ averaged normalized plasma density of the inhomogeneous e^-/e^+ plasma along the $\hat{x}$ direction at different simulation time settings. Plasma density is normalized by the mean upstream plasma density.

$t \sim 200\omega_{pe}^{-1}$ represents the shock transition region. The electrons move toward the low-density region, rapidly increasing the number of electrons in the low-density region. The magenta line taken at $t \sim 400\omega_{pe}^{-1}$ shows the system reached to the equilibration stage, as supported by the temperature anisotropy calculations shown in Figure 4. It would be interesting to study the highly relativistic collisionless shock generation in an inhomogeneous e^-/e^+ plasma medium in future.

Conclusion

2D PIC simulation has been carried out for a counterstreaming electron–positron (e^-/e^+) plasma system having intrinsic temperature anisotropy with the homogeneous and inhomogeneous density distributions. Such types of distributions are relevant for the relative motions of filaments and expected to exist in astrophysical environments.

Our simulation results show that in a pre-existing, upstream homogeneous density fluctuations, the initial strong temperature anisotropy $T_y \gg T_x$ gradually drops with time and becomes zero (isotropized system) at the end of the simulation. Subsequently, the Weibel instability-driven magnetic field energy is amplified

exponentially up to ($\sim 10^{-1}$) in a linear stage and then decays gradually to post-saturation. However, in the case of pre-existing, upstream inhomogeneous density fluctuations, we find that the finite temperature anisotropy exists at post-saturation and the magnetic field is re-amplified ($t \sim 270\omega_{pe}^{-1}$) in the downstream region. The increase in the magnetic field in the downstream region can be larger depending on how strong is the inhomogeneity factor of the upstream density fluctuations. The hot particles are shifted to the low-density region from the high-density region, which causes temperature increment in the $\hat{x}$ direction resulting in the velocity dispersion. Therefore, the density fluctuations cause a finite temperature anisotropy and the magnetic field amplification in the downstream region. The upstream isotropic density structures are compressed by collisionless shock and made to be anisotropic density structures causing the temperature anisotropy in the downstream region. Weibel instability extracts free energy from the anisotropy of the particles, producing filamentary currents aligned with the normal, and these currents are responsible for the creation of transverse magnetic fields and its amplification in the magnetic energy. Hence, the generated magnetic fields cover large regions. This analysis can be applied to wide range scenarios of astrophysical plasmas such as supernova remnants and GRBs whereby pre-existing large-scale upstream turbulence causes the magnetic field amplification in the downstream region.

Acknowledgments. This work was supported by the National Research Foundation of Korea (NRF); the Ministry of Science, ICT and Future Planning (MSIP) (NRF-2016R1A5A1013277); and the CHEA project, Korea.

References

Arber TD, Bennett K, Brady CS, Lawrence-Douglas A, Ramsay MG, Sircombe NJ, Gillies P, Evans RG, Schmitz H, Bell AR and Ridgers CP (2015) Contemporary particle-in-cell approach to laser-plasma modelling. *Plasma Physics and Controlled Fusion* **57**, 113001.

Ardaneh K, Cai D, Nishikawa KI and Lembege B (2015) Collisionless Weibel shocks and electron acceleration in gamma-ray bursts. *The Astrophysical Journal* **811**, 57.

Armstrong JW, Cordes JM and Rickett BJ (1981) Density power spectrum in the local interstellar medium. *Nature* **291**, 561–564.

Armstrong JW, Rickett BJ and Spangler SR (1995) Electron density power spectrum in the local interstellar medium. *The Astrophysical Journal* **443**, 209.

Bamba A, Yamazaki R, Yoshida T, Terasawa T and Koyama K (2005) A spatial and spectral study of nonthermal filaments in historical supernova remnants: observational results with Chandra. *The Astrophysical Journal* **621**, 793.

Bell AR (2004) Turbulent amplification of magnetic field and diffusive shock acceleration of cosmic rays. *Monthly Notices of the Royal Astronomical Society* **353**, 550.

Berezhko EG, Puhlhofer G and Volk HJ (2003*a*) Gamma-ray emission from Cassiopeia A produced by accelerated cosmic rays. *Astronomy and Astrophysics* **400**, 971.

Berezhko EG, Ksenofontov LT and Volk HJ (2003*b*) Confirmation of strong magnetic field amplification and nuclear cosmic ray acceleration in SN 1006. *Astronomy and Astrophysics* **412**, L11.

Bret A (2006) A simple analytical model for the Weibel instability in the non-relativistic regime. *Physics Letters A* **359**, 52.

Bret A and Deutsch C (2006) Stabilization of the filamentation instability and the anisotropy of the background plasma. *Physics of Plasmas* **13**, 022110.

Bret A, Stockem AN and Narayan R (2016) Theory of the formation of a collisionless weibel shock: pair vs. electron/proton plasmas. *Laser and Particle Beams* **34**, 362.

Califano F, Pegoraro F, Bulanov SV and Mangeney A (1998) Kinetic saturation of the Weibel instability in a collisionless plasma. *Physical Review E* **57**, 7048.

Cho M-H, Kim Y-K, Suk H, Ersfeld B, Jaroszynski DA and Hur MS (2015) Strong terahertz emission from electromagnetic diffusion near cutoff in plasma. *New Journal of Physics* **17**, 043045.

Davidson RC, Hammer DA, Haber I and Wagner CE (1972) Nonlinear development of electromagnetic instabilities in anisotropic plasmas. *Physics of Fluids* **15**, 317.

Dieckmann ME and Bret A (2017) Simulation study of the formation of a non-relativistic pair shock. *Journal of Plasma Physics* **83**, 905830104.

Dieckmann ME and Bret A (2018) Electrostatic and magnetic instabilities in the transition layer of a collisionless weakly relativistic pair shock. *Monthly Notices of the Royal Astronomical Society* **473**, 198.

Fiuza F, Fonseca RA, Tonge J, Mori WB and Silva LO (2012) Weibel-instability-mediated collisionless shocks in the laboratory with ultraintense lasers. *Physical Review Letters* **108**, 235004.

Fox W, Fiksel G, Bhattacharjee A, Chang PY, Germaschewski K, Hu SX and Nilson PM (2013) Filamentation instability of counterstreaming laser-driven plasmas. *Physical Review Letters* **111**, 225002.

Fried BD (1959) Mechanism for instability of transverse plasma waves. *Physics of Fluids* **2**, 337.

Fried BD and Conte SD (1961) *The Plasma Dispersion Function*. New York: Academic Press.

Grassi A, Grech M, Amiranoff F, Pegoraro F, Macchi A and Riconda C (2017) Electron Weibel instability in relativistic counterstreaming plasmas with flow-aligned external magnetic fields. *Physical Review E* **95**, 023203.

Hur MS and Suk H (2011) Numerical study of 1.1 GeV electron acceleration over a-few-millimeter-long plasma with a tapered density. *Physics of Plasmas* **18**, 033102.

Kalman G, Montes C and Quemada D (1968) Anisotropic temperature plasma instabilities. *Physics of Fluids* **11**, 1797.

Kronberg P (2002) Intergalactic magnetic fields. *Physics Today* **55**, 1240.

Lazar M (2008) Fast magnetization in counterstreaming plasmas with temperature anisotropies. *Physics Letters A* **372**, 2446.

Lazar M, Schlickeiser R and Shukla PK (2006) Cumulative effect of the filamentation and Weibel instabilities in counterstreaming thermal plasmas. *Physics of Plasmas* **13**, 102107.

Lazar M, Schlickeiser R and Shukla PK (2008) Cumulative effect of the Weibel-type instabilities in symmetric counterstreaming plasmas with kappa anisotropies. *Physics of Plasmas* **15**, 042103.

Lazar M, Schlickeiser R, Wielebinski R and Poedts S (2009*a*) Cosmological effects of Weibel-type instabilities. *The Astrophysical Journal* **693**, 1133.

Lazar M, Smolyakov A, Schlickeiser R and Shukla PK (2009*b*) A comparative study of the filamentation and Weibel instabilities and their cumulative effect. I. Non-relativistic theory. *Journal of Plasma Physics* **75**, 19.

Lee LC and Jokipii JR (1976) The irregularity spectrum in interstellar space. *The Astrophysical Journal* **206**, 735–743.

Lucek SG and Bell AR (2000) Non-linear amplification of a magnetic field driven by cosmic ray streaming. *Monthly Notices of the Royal Astronomical Society* **314**, 65.

Medvedev MV and Loeb A (1999) Generation of magnetic fields in the relativistic shock of gamma-ray burst sources. *The Astrophysical Journal* **526**, 697.

Medvedev MV, Fiore M, Fonseca RA, Silva LO and Mori WB (2005) Long-time evolution of magnetic fields in relativistic gamma-ray burst shocks. *Astrophysical Journal Letters* **618**, L75.

Niemiec J, Pohl M, Stroman T and Nishikawa KI (2008) Production of magnetic turbulence by cosmic rays drifting upstream of supernova remnant shocks. *The Astrophysical Journal* **684**, 1174–1189.

Nishikawa KI, Hardee P, Richardson G, Preece R, Sol H and Fishman GJ (2003) Particle acceleration in relativistic jets due to Weibel instability. *The Astrophysical Journal* **595**, 555.

Ohira Y, Reville B, Kirk JG and Takahara F (2009) Two-dimensional particle-in-cell simulations of the nonresonant, cosmic-ray driven instability in SNR shocks. *The Astrophysical Journal* **698**, 445.

Reville B, Kirk JG and Duffy P (2006) A current-driven instability in parallel, relativistic shocks. *Plasma Physics and Controlled Fusion* **48**, 1741.

Reville B, Kirk JG, Duffy PD and O'Sullivan S (2007) A cosmic ray current-driven instability in partially ionised media. *Astronomy and Astrophysics* **475**, 435–439.

Riquelme MA and Spitkovsky A (2008) Kinetic simulations of the current-driven instability in cosmic ray modified relativistic shocks. *International Journal of Modern Physics D* **17**, 1803.

Rowlands G, Dieckmann ME and Shukla PK (2007) The plasma filamentation instability in one dimension: nonlinear evolution. *New Journal of Physics* **9**, 247.

Silva LO, Fonseca RA, Tonge JW, Mori WB and Dawson JM (2002) On the role of the purely transverse Weibel instability in fast ignitor scenarios. *Physics of Plasmas* **9**, 2458.

Sironi L and Goodman J (2007) Production of magnetic energy by macroscopic turbulence in GRB afterglows. *The Astrophysical Journal* **671**, 1858.

Spitkovsky A (2008) On the structure of relativistic collisionless shocks in electron-ion plasmas. *Astrophysical Journal Letters* **673**, L39.

Stockem A and Lazar M (2008) Revision of cumulative effect of the filamentation and Weibel instabilities in counterstreaming thermal plasmas. *Physics of Plasmas* **15**, 014501.

Stockem A, Lazar M, Shukla PK and Smolyakov A (2009) A comparative study of the filamentation and Weibel instabilities and their cumulative effect. II. Weakly relativistic beams. *Journal of Plasma Physics* **75**, 529.

Tomita S and Ohira Y (2016) Weibel instability driven by spatially anisotropic density structures. *The Astrophysical Journal* **825**, 103.

Uchiyama Y, Aharonian T, Tanaka T, Takahashi T and Maeda Y (2007) Extremely fast acceleration of cosmic rays in a supernova remnant. *Nature* **449**, 576.

Vink J and Laming JM (2003) On the magnetic fields and particle acceleration in Cassiopeia A. *The Astrophysical Journal* **584**, 758.

Weibel ES (1959) Spontaneously growing transverse waves in a plasma due to an anisotropic velocity distribution. *Physical Review Letters* **2**, 83.